AGU PUBLICATIONS

JGR

Journal of Geophysical Research: Biogeosciences

BRIEF REPORT

10.1002/2013JG002460

Key Points:
- Compare camera phenological metrics to weekly leaf properties along whole season
- Observed mismatch between canopy greenness and leaf chlorophyll in the spring
- Vegetation senescence can be quantified from camera redness in the fall.

Supporting Information:
- Readme
- Figure S1

Correspondence to:
J. Tang,
jtang@mbl.edu

Citation:
Yang, X., J. Tang, and J. F. Mustard (2014), Beyond leaf color: Comparing camera-based phenological metrics with leaf biochemical, biophysical, and spectral properties throughout the growing season of a temperate deciduous forest, *J. Geophys. Res. Biogeosci.*, *119*, 181–191, doi:10.1002/2013JG002460.

Received 26 JUL 2013
Accepted 10 JAN 2014
Accepted article online 18 JAN 2014
Published online 31 MAR 2014

Beyond leaf color: Comparing camera-based phenological metrics with leaf biochemical, biophysical, and spectral properties throughout the growing season of a temperate deciduous forest

Xi Yang[1,2], Jianwu Tang[2,1], and John F. Mustard[1]

[1]Department of Geological Sciences, Brown University, Providence, Rhode Island, USA, [2]The Ecosystems Center, Marine Biological Laboratory, Woods Hole, Massachusetts, USA

Abstract Plant phenology, a sensitive indicator of climate change, influences vegetation-atmosphere interactions by changing the carbon and water cycles from local to global scales. Camera-based phenological observations of the color changes of the vegetation canopy throughout the growing season have become popular in recent years. However, the linkages between camera phenological metrics and leaf biochemical, biophysical, and spectral properties are elusive. We measured key leaf properties including chlorophyll concentration and leaf reflectance on a weekly basis from June to November 2011 in a white oak forest on the island of Martha's Vineyard, Massachusetts, USA. Concurrently, we used a digital camera to automatically acquire daily pictures of the tree canopies. We found that there was a mismatch between the camera-based phenological metric for the canopy greenness (green chromatic coordinate, g_{cc}) and the total chlorophyll and carotenoids concentration and leaf mass per area during late spring/early summer. The seasonal peak of g_{cc} is approximately 20 days earlier than the peak of the total chlorophyll concentration. During the fall, both canopy and leaf redness were significantly correlated with the vegetation index for anthocyanin concentration, opening a new window to quantify vegetation senescence remotely. Satellite- and camera-based vegetation indices agreed well, suggesting that camera-based observations can be used as the ground validation for satellites. Using the high-temporal resolution dataset of leaf biochemical, biophysical, and spectral properties, our results show the strengths and potential uncertainties to use canopy color as the proxy of ecosystem functioning.

1. Introduction

Plant phenology, the timing of periodic events in the life cycle of plants such as leaf out, flowering, and senescence, is a widely used indicator of climate change [*Rosenzweig et al*., 2007; *Walther et al*., 2002]. It is reported that leaf out and flowering in the Northern Hemisphere are advancing as a result of climate change [*Fitter and Fitter*, 2002; *Schwartz et al*., 2006; *Yang et al*., 2012]. These changes can exert feedback to the climate system through photosynthesis, canopy albedo, surface energy balance, canopy conductance, and emissions of volatile organic compounds [*Peñuelas et al*., 2009; *Richardson et al*., 2013]. Consequently, accurate characterization of vegetation phenology, especially the seasonal trajectories of key biophysical and biochemical properties (e.g., leaf area index and chlorophyll concentration), could improve the performance of terrestrial biosphere models [*Richardson et al*., 2012].

Plant phenology has been documented at different scales, including manual observations at the species level (<1 m^2) [e.g., *Richardson and O'Keefe*, 2009], remote sensing at regional and global scale (1–10 km^2 per pixel) [*Elmore et al*., 2012; *Fisher et al*., 2006; *Yang et al*., 2012; *Zhang et al*., 2003], and near-surface remote sensing of leaf phenology using digital cameras at the ecosystem scale (10–1000 m^2) [*Hufkens et al*., 2012; *Richardson et al*., 2009]. Digital cameras record the color changes of the vegetation canopy as an indicator of vegetation phenology. However, leaf reflectance in the visible and near-infrared bands may not be an accurate proxy for the plant physiology and biochemistry, as the physiological changes (e.g., photosynthetic capacity) could occur even when the leaf color is constant [*Bauerle et al*., 2012]. Leaf biochemical and biophysical properties, such as leaf nitrogen content, leaf chlorophyll and carotenoids concentration, and leaf mass per area, are directly related to the plant physiology. For example, nitrogen and chlorophyll are both key components in

plant photosynthesis [*Chapin et al*., 2011; *Wright et al*., 2004]; carotenoids protect leaves from environmental stress [*Demmig-Adams and Adams*, 2002]; and leaf mass per area measures the investment of plant dry mass per leaf area and is usually related to the rate of photosynthesis [*Poorter et al*., 2009]. Thus, field measurements of key leaf properties are necessary to understand whether and how leaf color change are related to plant physiological change during the growing season.

Leaf biophysical and biochemical properties change throughout the season, so do the leaf spectral properties [*Zhang et al*., 2007]. Traditional phenological observations focus on several phenological stages such as leaf out and flowering while ignoring the change during the growing season. However, climate-induced phenological shift could potentially affect not just the start and end of the growing season but also the midseason when ecosystem productivity has been considered to be relatively constant [*Richardson et al*., 2010]. In addition, some of the changes in leaf properties happen within weeks [e.g., *Jurik*, 1986]. Thus, a high-temporal resolution (~1 week) data set of these properties is critical for understanding the plant physiological processes and the camera-based phenological metrics.

Recently, given the relative simplicity of installing and maintaining digital cameras for automatically monitoring vegetation phenology, camera-based phenological observation is emerging as a mainstream approach (e.g., in NEON [*Keller et al*., 2008], PhenoCam [*Richardson et al*., 2009], and ICOS (Integrated Carbon Observation System, http://www.icos-infrastructure.eu)). Therefore, it is important to examine the physiological meanings of the phenological metrics derived from camera images. In this study, we aim to integrate the phenological observations at leaf, canopy, and satellite levels. Specifically, our objectives are to (1) understand the relationship between canopy-level camera phenological metrics and relevant leaf physiological properties and (2) examine the relationship between camera phenological metrics and remote sensing data.

2. Materials and Methods

2.1. Site Description

The study site (41°21′42.6″N, 70°34′41.7″W) was a deciduous white oak (*Quercus alba*) dominated forest located in the Manuel F. Correllus State Forest on the island of Martha's Vineyard, Massachusetts, U.S. The forest age was 80–115 years after natural recovery from abandoned cropland and pasture [*Foster et al*., 2002]. Mean temperatures were 20°C in the summer and 0°C in the winter, and annual precipitation was about 1200 mm from 1981 to 2010 (retrieved from National Climate Data Center: http://www.ncdc.noaa.gov).

2.2. Digital Camera Observations of Plant Phenology

Ground-based observations of plant phenology were documented with a north facing digital camera (Netcam MP, Stardot Inc., Buena Park, CA, U.S.) that was mounted with 15° downward view from the horizontal plane on top of a 15 meters tower (~10 meters above the canopy). The camera took pictures hourly from 10 A.M. to 3 P.M. every day from April to November 2011, and images were stored in a USB network storage system (TS-U100, Trendnet, Torrance, CA, USA). The system was powered by an 85 W solar panel (Suntech STP085B-12/BEA, Suntech, San Francisco, CA, USA) and two deep cycle batteries that were attached to an electrical timer (GE 15079, General Electric, Fairfield, CT, USA) that powered down the system during inactive periods for energy conservation.

Images from the camera system described above were processed in three steps. First, images where tree canopies are indiscernible because of rain drops on the protection case, heavy fog, and overexposed sky were identified manually and excluded from further analysis. Second, green and red chromatic coordinates (g_{cc} and r_{cc}, *Gillespie et al*. [1987] and *Sonnentag et al*. [2012]) for each image were calculated as the averaged g_{cc} and r_{cc} of all the pixels within the region of interest (ROI), which contains most of the tree canopies in the picture (Figure 1). Calculated from every image (equation (1)) were g_{cc} and r_{cc} as follows:

$$g_{cc} = G/(R+G+B)$$
$$r_{cc} = R/(R+G+B) \quad (1)$$

where R, G, and B are red, green, and blue layer of the JPEG image. Leaf biochemical properties such as chlorophyll concentration and biophysical properties such as leaf mass per area (LMA) can affect the reflectance in the visible wavelength, including R, G, and B and thus could potentially be linked to g_{cc} and r_{cc} [*Asner et al*., 2009]. Third, we calculated the ninetieth percentile of all the values within a 3 day moving window based on the method of *Sonnentag et al*. [2012]. By doing so, we acquired the smoothed time series of g_{cc} and r_{cc} (Figure 2a).

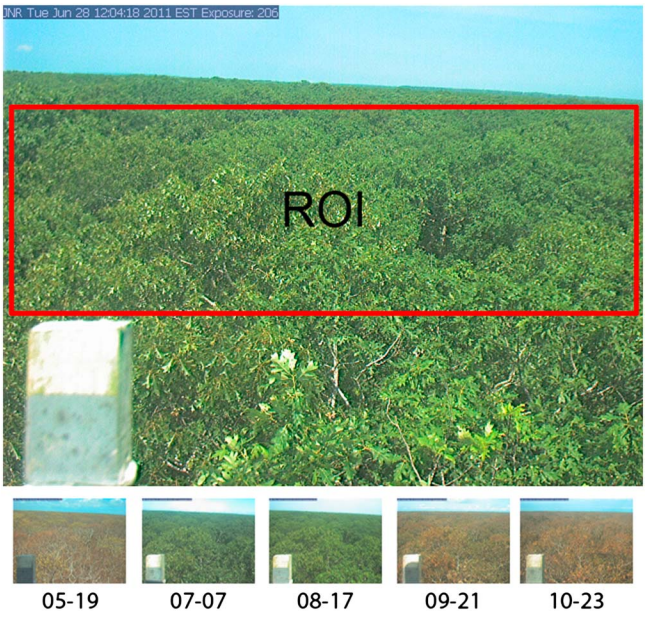

Figure 1. An example of the images acquired by the digital camera. The red rectangle indicates the region of interest (ROI) used to calculate camera phenological metrics such as green chromatic coordinate (g_{cc}). (bottom) Images from different times of the year (time format: mm-dd).

2.3. Leaf Spectral, Biophysical, and Biochemical Properties

A high-temporal resolution dataset of leaf spectral, biophysical, and biochemical properties was collected. The weekly (biweekly in August) sampling of leaves throughout the growing season (June 2011 to November 2011) was conducted on three white oak trees located within 5 m of the camera tower. For each sampling period, two fully sunlit branches (each having ~6 leaves) were randomly cut from each tree using a tree pruner and then immediately placed in a plastic bag containing a moist paper towel. All the samples were stored in a cooler filled with ice to keep the leaves from desiccation [*Foley et al*., 2006].

Each branch was divided into two subsets. One subset (3 leaves) was immediately used for leaf reflectance measurements in the field with a spectroradiometer (FS-3, Analytical Spectral Devices, Inc. Boulder, CO, U.S.; spectral range: 300–2500 nm, spectral resolution: 3 nm@700 nm, 10 nm@1400/2100 nm) and an integrating sphere (ASD Inc.). Each leaf spectrum was the average of 50 measurements. At least six leaf disks (~0.2827 cm^2 each) from the same subset of leaves were taken from each leaf using a hole puncher and then kept in the dry ice for the pigment analyses. Back in the lab, three leaf disks were ground in a mortar with 100% acetone solution and MgO [*Asner et al*., 2009]. After an 8 min centrifugation, the absorbance of the supernatant was measured using a spectrophotometer (Shimadzu UV-1201, Kyoto, Japan). Chlorophyll *a*, *b* and carotenoid concentrations were calculated using the readings from 470, 520, 645, 662, and 710 nm [*Lichtenthaler and Buschmann*, 2001]. The other subset (3 leaves) was scanned using a digital scanner (EPSON V300, EPSON, Long Beach, CA, U.S.), and oven dried (65°C) for at least 48 h for quantification of leaf dry mass. LMA was calculated based on the following equations:

$$\mathrm{LMA} = W_{\mathrm{dry}}/A_{\mathrm{leaf}} \tag{2}$$

where W_{dry} is leaf dry mass weight, A_{leaf} is the leaf area calculated from the scanned leaf using ImageJ [*Schneider et al*., 2012]. Dried leaves were then ground and analyzed for nitrogen percentage of dry mass (%N) with a CHNS/O analyzer (FLASH 2000, Thermo Scientific, Waltham, MA, U.S.).

The narrowband (<10 nm) leaf spectra were convoluted to produce broadband (the bandwidth is usually 30–100 nm for Moderate Resolution Imaging Spectroradiometer (MODIS)) reflectance using the spectral response functions (f_s) from the digital camera and MODIS (Table 1). The convolution from narrowband (R_N) to broadband (R_B) reflectance can be described as [*Liang*, 2003]:

$$R_B = \frac{\sum_{\lambda_{\min}}^{\lambda_{\max}} R_N(\lambda) f_s(\lambda)}{\sum_{\lambda_{\min}}^{\lambda_{\max}} f_s(\lambda)} \tag{3}$$

where λ is the wavelength (nm). Broadband red, green, and blue reflectances from the leaves were calculated to simulate the signal from leaves as received by the camera. Similarly, red, green, blue, and near-infrared (NIR hereafter) were calculated using the MODIS spectral response function and were then used to calculate normalized difference vegetation index (NDVI) and enhanced vegetation index (EVI) [*Huete et al*., 2002; *Sims and Gamon*, 2002]. We used three vegetation indices (anthocyanin reflectance index, ARI; modified anthocyanin reflectance index, mARI; and red:green ratio, RGR) as indicators of the anthocyanin

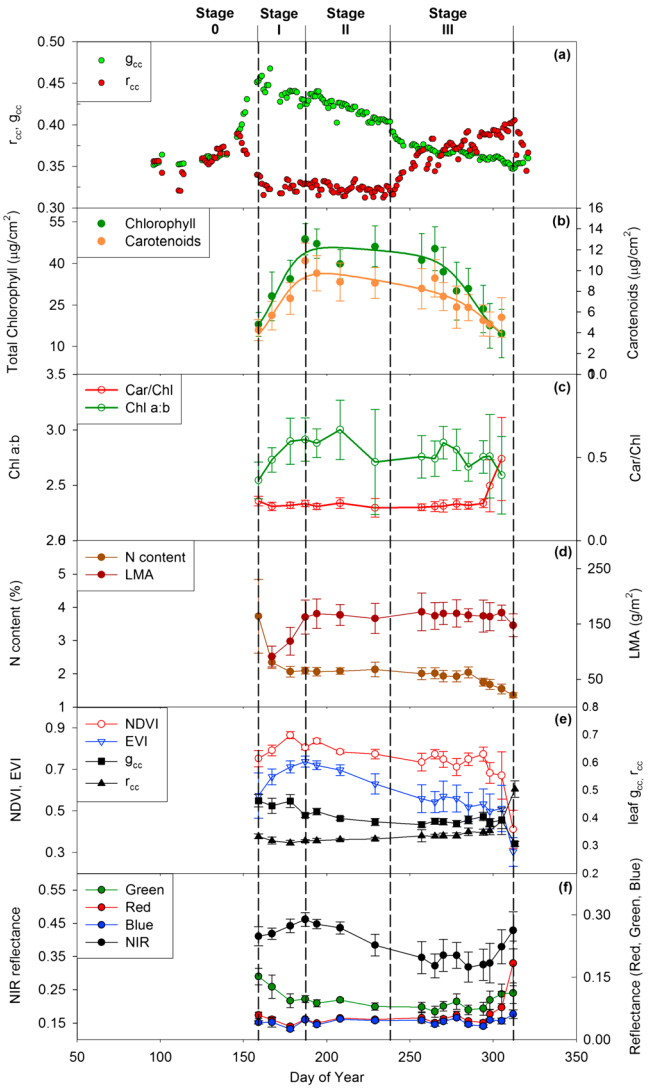

Figure 2. Comparisons between leaf biochemical, biophysical, and spectral properties and camera-based metrics. (a) Green chromatic coordinate (g_{cc}) and red chromatic coordinate (r_{cc}) calculated from camera time series. (b) Leaf total chlorophyll and carotenoids concentration (μg/cm^2). Solid dots are average from the 18 leaves sampled each time. The whiskers are the standard deviations; (c) Car/chl ratio and chl *a*/*b* ratio. (d) Mass-based total nitrogen content (%N), leaf mass per area (LMA). (e) Normalized difference vegetation index (NDVI), enhanced vegetation index (EVI), g_{cc} (green chromatic coordinate), and r_{cc} (red chromatic coordinate) calculated from leaf spectra; (f) green, red, near-infrared, and blue reflectance from the leaf spectra, see section 2.3 for details.

concentration in the leaves [*Gitelson et al.*, 2006; *Sims and Gamon*, 2002; *Ustin et al.*, 2009]. Using the scanned images of the leaves, we calculated the scanned leaf g_{cc} and r_{cc}.

We randomly collected six branches and measured the reflectance of their surfaces. In addition, we measured the reflectance of two surface soil samples. The stem and soil spectra were used to calculate the corresponding g_{cc} (Figure 3a).

2.4. Satellite Data

Satellite data of the study area were used for comparison with the camera-derived indices. MODIS 8 day 500 m surface reflectance data (MOD09A1) of year 2011 were downloaded (http://modis-land.gsfc.nasa.gov/, tile no.: h12v04). The pixel where the camera tower was located was obtained, and the pixel covered a homogenous area in terms of plant phenology [*Fisher and Mustard*, 2007]. Quality control was conducted by using the quality assessment (QA) layers: only days that were indicated as ideal quality (00 in first two bits of QA of MOD09A1 and 0 in first bit of QA of MOD15A2) were included in the analysis. Savitzky-Golay filter was used to smooth the time series [*Chen et al.*, 2004].

2.5. Statistical Method

Pearson's partial correlation coefficient (PCC) was used to estimate the relative contribution of each individual band (R, G, and B) to the seasonal patterns of g_{cc} and r_{cc}, at both canopy level and leaf level [*Shipley*, 2002]. In this study, PCC is an estimate of partial correlation coefficient between individual band (e.g., R) and g_{cc} (or r_{cc}), controlling the effect of other individual bands. PCC takes the value between −1 and 1. The higher the absolute value is, the more important the individual band is to the patterns of g_{cc} or r_{cc}. PCC was calculated as follows:

$$\rho_{XZ,Y} = \frac{\rho_{XZ} - \rho_{XY}\rho_{ZY}}{\sqrt{(1-\rho_{XY}^2)(1-\rho_{ZY}^2)}} \tag{4}$$

$\rho_{XZ,Y}$ is PCC between X and Z, with other variables (i.e., Y) fixed. In this study, X (or Y) is each individual band, while Z could be g_{cc} or r_{cc}. The correlations between XY, XZ, and ZY are ρ_{XY}, ρ_{XZ}, and ρ_{ZY}, respectively. PCC was calculated using a commercial software package (MATLAB R2012b, The MathWorks Inc., Natick, MA, 2000).

Table 1. Broadband and Narrowband Reflectance Used for the Calculation of Vegetation Indices

Sensors	Reflectance (and Bandwidth[a])	Indices[b]
Digital camera	R (577–698 nm), G (494–585 nm), and B (411–505 nm)	$g_{cc} = G/(R+G+B)$; $r_{cc} = R/(R+G+B)$
MODIS	R (620–670 nm), G (459–479 nm), B (545–565 nm), NIR (841–876 nm)	NDVI = (NIR − R)/(NIR + R); EVI = 2.5 × (NIR − R)/(NIR + 6 × R − 7.5 × B + 1)
ASD	$\rho_{530-570}$ (530 ~ 570 nm), $\rho_{690-710}$ (690 ~ 710 nm), $\rho_{760-800}$ (760 ~ 800 nm)	mARI = $(1/\rho_{530-570} - 1/\rho_{690-710}) \times \rho_{760-800}$; ARI = $1/\rho_{550} - 1/\rho_{700}$; RGR = $\rho_{600-699}/\rho_{500-599}$

[a]Spectral response function for the camera was retrieved from http://s1.archive.theimagingsource.com/publications/sensors-ccd/icx205ak/0eeddde64522190fb3cd9076af716619/icx205ak.en_US.pdf (accessed on 28 November 2012) and spectral response function for MODIS was retrieved from http://mcst.gsfc.nasa.gov/calibration/parameters (accessed on 28 November 2012). The bandwidth of digital camera was estimated using a simple calculation of FWHM (full width at half maximum), which is based on the spectral response function of the band [*Liang*, 2003].

[b]g_{cc}: green chromatic coordinate; r_{cc}: red chromatic coordinate; NDVI: normalized difference vegetation index; EVI: enhanced vegetation index; mARI: modified anthocyanin reflectance index; ARI: anthocyanin reflectance index; RGR: red-to-green ratio.

3. Results

3.1. Seasonal Trajectories of Canopy-Level Indices

The digital camera recorded the seasonal trajectories of canopy greenness and redness. The typical seasonal patterns reported for deciduous forests were shown by g_{cc} and r_{cc} in our site [e.g., *Henneken et al*., 2013; *Richardson et al*., 2009]. We divided the entire growing season into four stages based on the trajectories of g_{cc} and leaf chlorophyll concentration (Figure 2). The g_{cc} trajectory consists of a rapid increase in the spring due to leaf out (Stage 0, Figures 2a and 3); a seasonal peak in the early summer followed by a rapid decline (Stage I); a gradual decline in the middle to late summer (Stage II), and a rapid decline of g_{cc} in the autumn (Stage III). The general seasonal pattern of r_{cc} was the opposite to g_{cc}. In the early spring r_{cc} reached a local peak. When 100% of the leaves on the tree changed to red color in the fall, r_{cc} was highest and lowest when the canopy was fully covered by green leaves. Although the seasonal cycles of g_{cc} and r_{cc} were inversely correlated over the course of the year, there were several important differences between r_{cc} and g_{cc} trajectories within the season. For example, after day of year (DOY) 160 (9 June 2011), g_{cc} started to decline gradually until DOY 237 (25 August 2011), while r_{cc} remained stable during this period. During DOY 240–310, g_{cc} exhibited another decline, while r_{cc} increased to its seasonal peak. The period after the spring, g_{cc} peak can be divided into three stages (Figure 2a). Stage I was the period during which the g_{cc} started a rapid decline after the seasonal peak. During this period, r_{cc} remained stable. Stage II was a gradual decline of g_{cc} and stable r_{cc}. Stage III was marked as

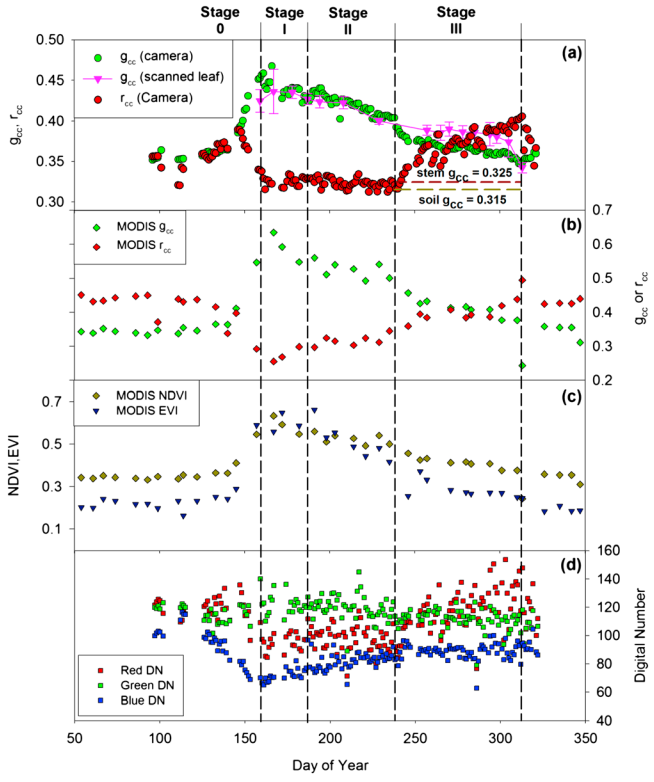

Figure 3. Comparisons of vegetation indices at the canopy level. (a) Green/red dots are g_{cc}/r_{cc} from digital camera. Pink triangles are g_{cc} calculated from scanned leaves. The whiskers are the standard deviation of 18 leaves each date. The horizontal dashed lines are g_{cc} of stem and soil calculated from spectra. (b) MODIS g_{cc} and r_{cc} calculated from the MOD09A1 reflectance product. (c) MODIS NDVI and EVI calculated from MOD09A1 product. (d) Raw digital number (DN) from red, green, and blue bands of digital camera images.

Table 2. Partial Correlation Coefficient (Pearson's Partial Correlation) Between Camera-Based g_{cc}/r_{cc} and Each Individual Band (R, G, B)[a]

		Stage 0	Stage I	Stage II	Stage III
g_{cc}	R	**−0.6843**	0.0509	0.1187	**−0.7710**
	G	**0.7265**	**0.5388**	**0.4817**	**0.6448**
	B	**−0.9266**	**−0.6748**	**−0.6894**	0.0691
r_{cc}	R	**0.9434**	**0.7595**	**0.8939**	**0.9664**
	G	**−0.7118**	**−0.5559**	**−0.6675**	**−0.5394**
	B	**−0.9149**	**−0.5142**	**−0.7005**	**−0.7962**

[a]Statistics in bold indicate that $p < 0.05$.

another gradual decline of g_{cc} and a rapid increase of r_{cc} to its seasonal peak. As both leaf- and canopy-level measurements overlap in these three stages, we focus the comparison (section 3.4) on Stage I–III.

The contribution of individual bands to canopy color varied at different stages (Table 2). The green and red were consistently important factors driving the seasonal changes of g_{cc} and r_{cc}, respectively. However, the blue band played a more important role for both g_{cc} and r_{cc} during certain stages. For example, the decline of blue in Stage 0 drove the increase in g_{cc}. Note that for camera data, the value for each individual band is the raw digital number, not necessarily reflecting the actual reflectance of each individual band.

The color as seen from the satellite showed a good agreement with that from the camera (Figure 3b). Overall, the agreement in g_{cc} between the satellite and camera was higher than that of the r_{cc} (MODIS versus camera, $r^2 = 0.878$ for g_{cc}, $r^2 = 0.531$ for r_{cc}). The three distinct stages similar to those in camera g_{cc} were observed in the MODIS g_{cc} time series. For g_{cc}, a spring peak and the following summer greendown was also obvious in the MODIS data. The spring local peak was not obvious in MODIS r_{cc} time series. However, a fall r_{cc} peak (and a g_{cc} minimum) was obvious in the MODIS r_{cc} time series.

We compared MODIS NDVI and EVI with the camera g_{cc} (Figure 3c). In stage I, NDVI reached its seasonal peak and started to decline, which is similar to that of the camera g_{cc}. However, EVI was stable or even increasing during this period. In stage II, like camera g_{cc}, NDVI and EVI both decreased. In stage III, there was another gradual decline of MODIS NDVI and EVI.

3.2. Seasonal Trajectories of Leaf Biochemical and Biophysical Properties

The seasonal trajectories of leaf biochemical and biophysical properties were similar to those in the previous research on deciduous trees [*Damesin*, 2003; *Jurik*, 1986; *Poorter et al*., 2009]. Area-based leaf total chlorophyll concentration (μg/cm^2) increased steadily in Stage I, reaching a plateau in Stage II, and gradually declined in Stage III (Figure 2b). The seasonal trajectory of area-based carotenoids concentration (μg/cm^2) was similar to that of the total chlorophyll. The only difference was in Stage II, when carotenoids started to decrease. The ratio between chlorophyll *a* and *b* (Chl *a*:*b*) generally varied between 2.5 and 3.0. During Stage I and early Stage II, Chl *a*:*b* increased to its seasonal peak at 3.0 and then was followed by a decrease to ~2.7 in Stage III (Figure 2c). The Carotenoids-to-Chlorophyll ratio (Car/Chl) was conservative through Stage I and II. In Stage III, a gradual increase of Car/Chl was followed by a rapid increase to the seasonal peak with a mean value of ~0.5.

The mean value of %N decreased from 4 to 2 in stage I (Figure 2d). After a stable Stage II, %N started to decrease during the end of Stage III, which presumably could be the result of nitrogen resorption during senescence [*Killingbeck*, 1996]. The seasonal trajectory of LMA is conservative compared to the other biochemical and biophysical properties (Figure 2d). LMA increased in Stage I to a plateau in Stage II and III and only showed a slight decrease by the end of the growing season.

3.3. Seasonal Trajectory of Vegetation Spectra

Leaf spectra at different times of the growing season exhibited distinct features (Figure 4). Each leaf biophysical and biochemical property contributes to different wavelengths of leaf spectra [*Jacquemoud and Baret*, 1990]. During the period between leaf budburst and maturity (May–August), the most significant change in the visible wavelength (VIS thereafter, 400 ~ 700nm) was the decrease of green reflectance (Figures 2f and 4). During the fall senescence, there was a sharp increase in the red reflectance, presumably caused by the decrease of total chlorophyll (Figure 2b). Similarly, there was a moderate increase of green reflectance.

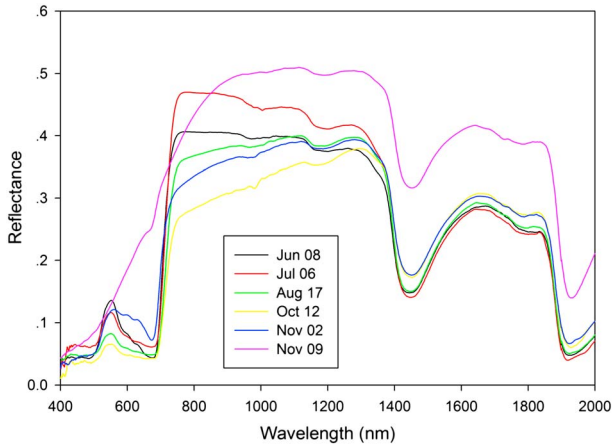

Figure 4. Examples of the leaf spectra (400 ~ 2000 nm) collected using ASD spectroradiometer throughout the season. Only a subsample of the spectra was plotted for the best visual effect. Curves in different colors represent leaf directional-hemispherical reflectance at different dates.

The contributions of each individual band (R, G, and B) from leaf spectra changed at different stages (Table 3). For g_{cc}, the green reflectance was the major contributor throughout the three stages. The green reflectance-g_{cc} relationship was significantly positive. The contribution of R to g_{cc} increased significantly throughout the season from nonsignificant (Stage I) to the dominant (Stage III). For r_{cc}, R was the major contributor. Blue also significantly affected the seasonal pattern of r_{cc} (Figures 2e and 2f). The green band contributed to the first two stages for r_{cc} but not the last stage.

NIR reflectance increased during DOY 159 ~ 187, which was followed by a gradual decrease till DOY 269 (26 September). After that, NIR reflectance increased until the end of the growing season (Figures 2f and 4). The spectra between 1300 nm and 2000 nm were conservative during most times of the season; only by the end of the season did reflectance in this region start to increase (Figure 4).

3.4. Comparisons Between Canopy Color and Leaf Biochemical, Biophysical, and Spectral Properties

Although both the canopy g_{cc} and the pigment concentrations showed a similar "bump" shape throughout the growing season, there were obvious discrepancies between the two types of time series. In stage I, while the g_{cc} started to decline from its annual peak, the total chlorophyll concentration in the leaves was still increasing (Figure 2b). At the same time, both carotenoids concentration and LMA increased, and the %N decreased. For leaf reflectance, an increase in the NIR (on average by 0.050) was accompanied by a decrease of R and G (on average by 0.029 and 0.040, respectively, Figures 2f and 4). Spectral indices such as NDVI and EVI showed an increase during this period.

Stage II is the "summer greendown." Between DOY 189 and 236, similar decreases of g_{cc} were observed at both canopy (Figure 3a) and leaf levels (Figure 2e). At the canopy level, g_{cc} gradually declines from 0.44 to 0.40 (~36% decrease compared to the seasonal amplitude). When taking the autocorrelation in data points into consideration [*Bence*, 1995], there is still a significant decline of carotenoids during Stage II ($p < 0.0001$) but no significant change of chlorophyll ($p = 0.159$). Similarly, there is a significant decline of EVI during this period. Both LMA and N content showed no significant change during this period.

Stage III is the "senescence" stage (DOY 237 ~ 311). Leaf-level r_{cc} was significantly correlated with the mARI ($r^2 = 0.635$, $p < 0.0001$), while for the entire growing season (including Stage I and II), the correlation was lower but still significant ($r^2 = 0.565$, $p < 0.0001$) (Figure 5). Although leaf-level g_{cc} and r_{cc} started to diverge from the canopy metrics (Figure 3a), there is still a significant correlation between the canopy r_{cc} and the

Table 3. Partial Correlation Coefficient (Pearson's Partial Correlation) Between Leaf-Level g_{cc}/r_{cc} and Each Individual Band (R, G, B)[a]

		Stage I	Stage II	Stage III
g_{cc}	R	−0.5426	**−0.7517**	**−0.9113**
	G	**0.8159**	**0.9788**	**0.8977**
	B	**−0.4300**	**−0.6730**	**−0.6822**
r_{cc}	R	**0.9285**	**0.9402**	**0.9445**
	G	**−0.7448**	**−0.7941**	**−0.0168**
	B	**−0.9087**	**−0.9217**	**−0.6441**

[a]Leaf-level reflectance in R, G, and B were calculated based on MODIS spectral response function using spectra collected by ASD spectrometer. Statistics in bold indicate that $p < 0.05$. Note that leaf spectra were collected since the beginning of Stage I.

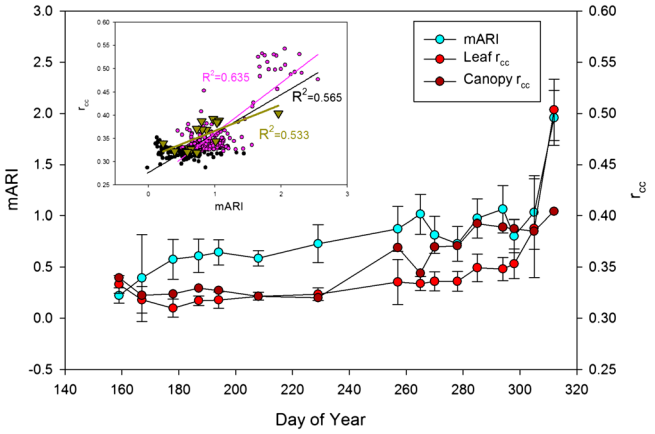

Figure 5. Comparisons of leaf- and canopy-level r_{cc} with modified anthocyanin reflectance index (mARI) throughout the growing season. The dots are mean values and the whiskers are standard deviations. The inset shows the scatterplot of entire growing season leaf r_{cc} ~ mARI (black dots + pink dots) and the linear regression (black line); Stage III only leaf r_{cc} ~ mARI (pink dots) and the linear regression (pink line); and canopy r_{cc} ~ mARI (dark yellow triangle) and the linear regression (dark yellow line).

median of leaf-level mARI ($r^2 = 0.533$, $p = 0.016$). Similarly, we found a good correlation between r_{cc} and the other two anthocyanin indices (Figure S1).

Both chlorophyll and carotenoids showed significant decrease at the senescence stage. The carotenoids/chlorophyll ratio shows a consistent increase during this period (on average from 0.201 to 0.497). LMA did not show significant decrease until ~ DOY 300. The %N content started to decrease at ~ DOY 285. During this period, NDVI and EVI all showed a consistent decline, while all three anthocyanin indices increased. Canopy g_{cc} decreased while r_{cc} increased to its seasonal peak.

4. Discussion

Aiming to examine the physiological meaning of camera-based phenological metrics in this study, we found a mismatch between camera-based canopy greenness and leaf biochemical and biophysical properties: in the spring, the seasonal peak of camera g_{cc} was approximately 20 days earlier than the peak of total chlorophyll and carotenoids concentration and LMA. During the fall, we found a significant correlation between the anthocyanin indices (mARI, ARI, and RGR) and r_{cc} at both canopy and leaf level.

Leaf biochemical and biophysical properties are major contributors to the amount of (1) the reflected solar radiation [*Asner and Martin*, 2008; *Jacquemoud et al*., 2009], the visible part of which is seen by digital camera and (2) the absorbed solar radiation by leaves, which is used for photosynthesis [*Demmig-Adams and Adams*, 2000; *Peng et al*., 2011]. Thus, we might expect that canopy colors (greenness or redness) show the same pattern as leaf pigmentation. However, the observed mismatch between canopy greenness and leaf biochemical properties suggests that the relationship between canopy color and leaf pigmentation is nonlinear. At the leaf level, pigments like chlorophyll and carotenoids are major contributors in the visible wavelength [*Asner*, 1998; *Jacquemoud and Baret*, 1990]. At the canopy level, leaf area index (LAI) (along with factors such as leaf inclination angle distribution) is considered to be the major contributor [*Asner and Martin*, 2008; *Jacquemoud et al*., 2009], especially with the oblique view of the digital camera, more layers of leaf can be seen, changing both the rate and magnitude of g_{cc} and r_{cc}. In Stage I and II, leaf-level g_{cc} matched well with canopy-level g_{cc}, indicating that leaf-level color change largely controlled the signal received by digital camera, though it is still possible that LAI could have an impact on the signal during these stages [*Samanta et al*., 2012]. During the fall, as leaves start to drop in Stage III, the signal received by the camera is from a mixture of leaves, branches, and background soil (Figure 3a). Thus, the leaf g_{cc} started to deviate from the camera g_{cc}, which is the averaged value from leaves with higher g_{cc} and branches/soil background with lower g_{cc}. The contribution of leaves to the canopy g_{cc} decreased during Stage III (Figure 3d). To disentangle the contributions of leaf chemistry and LAI, concurrent measurements of LAI from instruments like LAI-2000 can be helpful [*Gond et al*., 1999]. In addition, with the input of LAI and leaf biochemical, biophysical, and spectral properties, canopy radiative transfer models might be able to provide the mechanistic understanding for this mismatch [*Jacquemoud et al*., 2009].

At the leaf level, leaf biochemical and biophysical properties control the leaf color changes throughout the season. The decline of g_{cc} at Stage I was the result of greater decline of G, compared to the relatively stable R and B (Figure 2f and Table 3). Presumably, it can be explained by the change of leaf biochemical and biophysical properties: the increase of chlorophyll concentration is an indicator of leaf maturity, which is supported by the increase of LMA [*Ellsworth and Reich*, 1992; *Jurik*, 1986] and carotenoids concentration [*Lewandowska and Jarvis*, 1977], and the decline of the nitrogen concentration measured as the percentage

of dry weight [*Field and Mooney*, 1983; *Schultz et al*., 1982]. Could this mismatch simply be a result of the saturation of the g_{cc} as the pigments accumulate, like the saturation of NDVI as chlorophyll accumulates [*Gamon et al*., 1995]? Our results did not support this hypothesis. First, if g_{cc} saturates as the pigments accumulate in Stage I, g_{cc} should neither increase nor decrease as adding more pigments would have no effect. However, we observed a decline of g_{cc} at both leaf and canopy level. Second, there were significant increases in both NDVI and EVI during stage I, when chlorophyll increased. Both NDVI and EVI did not show saturation during this stage (data not shown).

Since total chlorophyll concentration is considered to be related to gross primary production (GPP), we might expect a similar mismatch between the canopy greenness and GPP in the spring [*Toomey et al*., 2012; *Xiao et al*., 2004], even though g_{cc} and GPP might have similar seasonal patterns [*Richardson et al*., 2009]. In addition, during Stage II, the leaf g_{cc} matched well with the canopy g_{cc}, showing the same decline in G (Figure 3a). This decline of g_{cc} was mainly controlled by the decrease of G (R and B were relatively constant (Table 2)) which could be attributed to leaf aging or potentially changes in leaf internal structure [*Slaton et al*., 2001] (as hinted by that NIR reflectance significantly declined during this period (Figure 2f)). Similarly, leaf-level NDVI and EVI all declined, but this "summer greendown" is rarely documented in remote sensing literatures [*Elmore et al*., 2012]. Leaf aging, paralleled with the decline of leaf photosynthetic capacity [*Wilson et al*., 2001], could affect GPP even though we see little change in chlorophyll concentration [*Bauerle et al*., 2012]. LMA did not correlate well with the change of canopy greenness. In the spring, the mismatch between canopy g_{cc} and LMA was similar to that between g_{cc} and chlorophyll concentration, presumably in Stage I leaves were still building up cell materials [*Poorter et al*., 2009].

The good correlation between camera and satellite-based g_{cc} time series suggests the potential to use digital cameras as the ground validation for satellites, for example, *Hufkens et al*. [2012] found a good match between satellite vegetation indices and canopy greenness (as indicated by another metric, ExG). However, our results suggest that the g_{cc} time series from both methods could mismatch with leaf pigmentations in the spring. In contrast, the r_{cc} and anthocyanin relationship could potentially be used to monitor fall senescence remotely just using reflectance at visible wavelength, at least in certain species with anthocyanin in the leaves [*Zhang and Goldberg*, 2011]. To further test the robustness of this observation, in situ measurements of leaf anthocyanin concentration can be helpful. To capture the seasonality of leaf physiology, ground-based measurements of leaf biochemical, biophysical, and spectral properties should complement near-surface and remote sensing data with high-temporal and spatial resolutions.

Acknowledgments

We thank Dennis Baldocchi, the associate editor and three anonymous reviewers for their constructive comments. We would like to thank Johanna Schmitt for the discussion and Adrian Rocha for commenting on an earlier version of this manuscript. We thank Katie Laushman, Lakiah Clark, Skyler Hackley, and Tim Savas for assisting with fieldwork. We thank Matthew Erickson, Marshall Otter, Rich McHorney, Jane Tucker, and Sam Kelsey for the help with lab work. We also thank the Manuel F. Correllus State Forest, the Nature Conservancy Hoft Farm Preserve, and Colbert for the permission to use the forests in the island of Martha's Vineyard in Massachusetts for our research. This research was supported by the Brown University–Marine Biological Laboratory graduate program in Biological and Environmental Sciences, Brown–ECI phenology working group, Brown Office of International Affairs Seed Grant on phenology, and Marine Biological Laboratory start-up funding for JT.

References

Asner, G. P. (1998), Biophysical and biochemical sources of variability in canopy reflectance, *Remote Sens. Environ.*, *64*(3), 234–487.

Asner, G., and R. Martin (2008), Spectral and chemical analysis of tropical forests: Scaling from leaf to canopy levels, *Remote Sens. Environ.*, *112*(10), 3958–3970.

Asner, G. P., R. E. Martin, A. Ford, D. Metcalfe, and M. Liddell (2009), Leaf chemical and spectral diversity in Australian tropical forests, *Ecol. Appl.*, *19*(1), 236–253.

Bauerle, W. L., R. Oren, D. A. Way, S. S. Qian, P. C. Stoy, P. E. Thornton, J. D. Bowden, F. M. Hoffman, and R. F. Reynolds (2012), Photoperiodic regulation of the seasonal pattern of photosynthetic capacity and the implications for carbon cycling, *Proc. Natl. Acad. Sci. U. S. A.*, *109*(22), 8612–8617.

Bence, J. R. (1995), Analysis of short time series: Correcting for autocorrelation, *Ecology*, *76*(2), 628–639.

Chapin, F. S., P. A. Matson, and P. M. Vitousek (2011), *Principles of Terrestrial Ecosystem Ecology*, 2nd ed., Springer, New York.

Chen, J., P. Jönsson, M. Tamura, Z. Gu, B. Matsushita, and L. Eklundh (2004), A simple method for reconstructing a high-quality NDVI time-series data set based on the Savitzky–Golay filter, *Remote Sens. Environ.*, *91*(3–4), 332–344.

Damesin, C. (2003), Respiration and photosynthesis characteristics of current-year stems of Fagus sylvatica: From the seasonal pattern to an annual balance, *New Phytol.*, *158*(3), 465–475.

Demmig-Adams, B., and W. W. Adams (2000), Photosynthesis: Harvesting sunlight safely, *Nature*, *403*(6768), 371–374.

Demmig-Adams, B., and W. W. Adams (2002), Antioxidants in photosynthesis and human nutrition, *Science*, *298*(5601), 2149–2153.

Ellsworth, D. S., and P. B. Reich (1992), Leaf mass per area, nitrogen content and photosynthetic carbon gain in *Acer saccharum* seedlings in contrasting forest light environments, *Funct. Ecol.*, *6*(4), 423–435.

Elmore, A. J., S. M. Guinn, B. J. Minsley, and A. D. Richardson (2012), Landscape controls on the timing of spring, autumn, and growing season length in mid-Atlantic forests, *Global Change Biol.*, *18*(2), 656–674.

Field, C., and H. A. Mooney (1983), Leaf age and seasonal effects on light, water, and nitrogen use efficiency in a California shrub, *Oecologia*, *56*(2), 348–355.

Fisher, J., and J. Mustard (2007), Cross-scalar satellite phenology from ground, Landsat, and MODIS data, *Remote Sens. Environ.*, *109*, 261–273.

Fisher, J., J. Mustard, and M. Vadboncoeur (2006), Green leaf phenology at Landsat resolution: Scaling from the field to the satellite, *Remote Sens. Environ.*, *100*, 265–279.

Fitter, A. H., and R. S. Fitter (2002), Rapid changes in flowering time in British plants, *Science*, *296*(5573), 1689–1691.

Foley, S., B. Rivard, G. Sanchez-Azofeifa, and J. Calvo (2006), Foliar spectral properties following leaf clipping and implications for handling techniques, *Remote Sens. Environ.*, *103*(3), 265–275.

Foster, D., B. Hall, S. Barry, S. Clayden, and T. Parshall (2002), Cultural, environmental and historical controls of vegetation patterns and the modern conservation setting on the island of Martha's Vineyard USA, *J. Biogeogr.*, *29*, 1381–1400.
Gamon, J. A., C. B. Field, M. L. Goulden, K. L. Griffin, A. E. Hartley, G. Joel, J. Peñuelas, and R. Valentini (1995), Relationships between NDVI, canopy structure, and photosynthesis in three Californian vegetation types, *Ecol. Appl.*, *5*, 28–41.
Gillespie, A. R., A. B. Kahle, and R. E. Walker (1987), Color enhancement of highly correlated images. II. Channel ratio and "chromaticity" transformation techniques, *Remote Sens. Environ.*, *22*(3), 343–365.
Gitelson, A. A., G. P. Keydan, and M. N. Merzlyak (2006), Three-band model for noninvasive estimation of chlorophyll, carotenoids, and anthocyanin contents in higher plant leaves, *Geophys. Res. Lett.*, *33*, L11402, doi:10.1029/2006GL026457.
Gond, V., D. G. G. de Pury, F. Veroustraete, and R. Ceulemans (1999), Seasonal variations in leaf area index, leaf chlorophyll, and water content; scaling-up to estimate fAPAR and carbon balance in a multilayer, multispecies temperate forest, *Tree physiology*, *19*(10), 673–679.
Henneken, R., V. Dose, C. Schleip, and A. Menzel (2013), Detecting plant seasonality from webcams using Bayesian multiple change point analysis, *Agric. For. Meteorol.*, *168*(0), 177–185.
Huete, A., K. Didan, T. Miura, E. P. Rodriguez, X. Gao, and L. G. Ferreira (2002), Overview of the radiometric and biophysical performance of the MODIS vegetation indices, *Remote Sens. Environ.*, *83*(1–2), 195–213.
Hufkens, K., M. Friedl, O. Sonnentag, B. H. Braswell, T. Milliman, and A. D. Richardson (2012), Linking near-surface and satellite remote sensing measurements of deciduous broadleaf forest phenology, *Remote Sens. Environ.*, *117*(0), 307–321.
Jacquemoud, S., and F. Baret (1990), PROSPECT: A model of leaf optical properties spectra, *Remote Sens. Environ.*, *34*(2), 75–91.
Jacquemoud, S., W. Verhoef, F. Baret, C. Bacour, P. J. Zarco-Tejada, G. P. Asner, C. François, and S. L. Ustin (2009), PROSPECT + SAIL models: A review of use for vegetation characterization, *Remote Sens. Environ.*, *113*(1), S56–S66.
Jurik, T. W. (1986), Temporal and spatial patterns of specific leaf weight in successional northern hardwood tree species, *Am. J. Bot.*, *73*(8), 1083–1092.
Keller, M., D. Schimel, W. W. Hargrove Jr., and F. M. Hoffman (2008), A continental strategy for the National Ecological Observatory Network (NEON), *Front. Ecol. Environ.*, *6*(5), 282–284.
Killingbeck, K. T. (1996), Nutrients in Senesced leaves: Keys to the search for potential resorption and resorption proficiency, *Ecology*, *77*(6), 1716–1727.
Lewandowska, M., and P. Jarvis (1977), Changes in chlorophyll and carotenoid content, specific leaf area and dry weight fraction in Sitka spruce, in response to shading and season, *New Phytol.*, *79*(2), 247–256.
Liang, S. (2003), *Quantitative Remote Sensing of Land Surfaces*, Wiley-Interscience, Hoboken, NJ, America.
Lichtenthaler, H. K., and C. Buschmann (2001), Chlorophylls and carotenoids: Measurement and characterization by UV–VIS spectroscopy, in *Current Protocols in Food Analytical Chemistry*, pp. 705–758, John Wiley, New York.
Peng, Y., A. A. Gitelson, G. Keydan, D. C. Rundquist, and W. Moses (2011), Remote estimation of gross primary production in maize and support for a new paradigm based on total crop chlorophyll content, *Remote Sens. Environ.*, *115*(4), 978–989.
Peñuelas, J., T. Rutishauser, and I. Filella (2009), Phenology feedbacks on climate change, *Science*, *324*(5929), 887–888.
Poorter, H., Ü. Niinemets, L. Poorter, I. J. Wright, and R. Villar (2009), Causes and consequences of variation in leaf mass per area (LMA): A meta-analysis, *New Phytol.*, *182*(3), 565–588.
Richardson, A. D., and J. O'Keefe (2009), Phenological differences between understory and overstory: A case study using the long-term Harvard Forest records, in *Phenology of Ecosystem Processes*, edited by A. Noormets, pp. 87–117, Springer Science, New York.
Richardson, A. D., B. Braswell, D. Hollinger, J. Jenkins, and S. Ollinger (2009), Near-surface remote sensing of spatial and temporal variation in canopy phenology, *Ecol. Appl.*, *19*(6), 1417–1428.
Richardson, A. D., et al. (2010), Influence of spring and autumn phenological transitions on forest ecosystem productivity, *Philos. Trans. R. Soc. B: Biological Sciences*, *365*(1555), 3227–3246.
Richardson, A. D., et al. (2012), Terrestrial biosphere models need better representation of vegetation phenology: Results from the North American Carbon Program Site Synthesis, *Global Change Biol.*, *18*(2), 566–584.
Richardson, A. D., T. F. Keenan, M. Migliavacca, Y. Ryu, O. Sonnentag, and M. Toomey (2013), Climate change, phenology, and phenological control of vegetation feedbacks to the climate system, *Agric. For. Meteorol.*, *169*(0), 156–173.
Rosenzweig, C., G. Casassa, D. J. Karoly, A. Imeson, C. Liu, A. Menzel, S. Rawlins, T. L. Root, B. Seguin, and P. Tryjanowski (2007), Assessment of observed changes and responses in natural and managed systems, in *Climate Change 2007: Impacts, Adaptation and Vulnerability. Contribution of Working Group II to the Fourth Assessment Report of the Intergovernmental Panel on Climate Change*, edited by M. L. Parry et al., pp. 79–131, Cambridge Univ. Press, Cambridge, U. K.
Samanta, A., Y. Knyazikhin, L. Xu, R. E. Dickinson, R. Fu, M. H. Costa, S. S. Saatchi, R. R. Nemani, and R. B. Myneni (2012), Seasonal changes in leaf area of Amazon forests from leaf flushing and abscission, *J. Geophys. Res.*, *117*, G01015, doi:10.1029/2011JG001818.
Schneider, C. A., W. S. Rasband, and K. W. Eliceiri (2012), NIH Image to ImageJ: 25 years of image analysis, *Nat. Methods*, *9*(7), 671–675.
Schultz, J. C., P. J. Nothnagle, and I. T. Baldwin (1982), Seasonal and individual variation in leaf quality of two northern hardwoods tree species, *Am. J. Bot.*, *69*(5), 753–759.
Schwartz, M. D., R. Ahas, and A. Aasa (2006), Onset of spring starting earlier across the Northern Hemisphere, *Global Change Biol.*, *12*(2), 343–351.
Shipley, B. (2002), *Cause and Correlation in Biology: A User's Guide to Path Analysis Structural Equations and Causal Inference*, Cambridge Univ. Press, Cambridge.
Sims, D. A., and J. A. Gamon (2002), Relationships between leaf pigment content and spectral reflectance across a wide range of species, leaf structures and developmental stages, *Remote Sens. Environ.*, *81*(2–3), 337–354.
Slaton, M. R., E. Raymond Hunt, and W. K. Smith (2001), Estimating near-infrared leaf reflectance from leaf structural characteristics, *Am. J. Bot.*, *88*(2), 278–284.
Sonnentag, O., K. Hufkens, C. Teshera-Sterne, A. M. Young, M. Friedl, B. H. Braswell, T. Milliman, J. O'Keefe, and A. D. Richardson (2012), Digital repeat photography for phenological research in forest ecosystems, *Agric. For. Meteorol.*, *152*(0), 159–177.
Toomey, M. P., M. A. Friedl, K. Hufkens, O. Sonnentag, T. E. Milliman, S. Frolking, and A. D. Richardson (2012), Monitoring of phenological control on ecosystem fluxes using digital cameras and eddy covariance data, American Geophysical Union Fall Meeting, San Francisco.
Ustin, S. L., A. A. Gitelson, S. Jacquemoud, M. Schaepman, G. P. Asner, J. A. Gamon, and P. Zarco-Tejada (2009), Retrieval of foliar information about plant pigment systems from high resolution spectroscopy, *Remote Sens. Environ.*, *113*(Supplement 1), S67–S77.
Walther, G.-R., E. Post, P. Convey, A. Menzel, C. Parmesan, T. J. C. Beebee, J.-M. Fromentin, O. Hoegh-Guldberg, and F. Bairlein (2002), Ecological responses to recent climate change, *Nature*, *416*(6879), 389–395.
Wilson, K. B., D. D. Baldocchi, and P. J. Hanson (2001), Leaf age affects the seasonal pattern of photosynthetic capacity and net ecosystem exchange of carbon in a deciduous forest, *Plant Cell Environ.*, *24*(6), 571–583.

Wright, I. J., et al. (2004), The worldwide leaf economics spectrum, *Nature*, *428*(6985), 821–827.
Xiao, X., Q. Zhang, B. Braswell, S. Urbanski, S. Boles, S. Wofsy, B. Moore Iii, and D. Ojima (2004), Modeling gross primary production of temperate deciduous broadleaf forest using satellite images and climate data, *Remote Sens. Environ.*, *91*(2), 256–270.
Yang, X., J. F. Mustard, J. Tang, and H. Xu (2012), Regional-scale phenology modeling based on meteorological records and remote sensing observations, *J. Geophys. Res.*, *117*, G03029, doi:10.1029/2012JG001977.
Zhang, X., and M. D. Goldberg (2011), Monitoring fall foliage coloration dynamics using time-series satellite data, *Remote Sens. Environ.*, *115*(2), 382–391.
Zhang, X., M. Friedl, C. Schaaf, A. Strahler, J. Hodges, F. Gao, B. Reed, and A. Huete (2003), Monitoring vegetation phenology using MODIS, *Remote Sens. Environ.*, *84*, 471–475.
Zhang, Y., J. M. Chen, and S. C. Thomas (2007), Retrieving seasonal variation in chlorophyll content of overstory and understory sugar maple leaves from leaf-level hyperspectral data, *Can. J. Remote Sens.*, *33*(5), 406–415.